Available online at www.sciencedirect.com
ScienceDirect
Biochimica et Biophysica Acta 1768 (2007) 467–478
Biochimica et Biophysica Acta BBA
www.elsevier.com/locate/bbamem

Location and dynamics of acyl chain NBD-labeled phosphatidylcholine (NBD-PC) in DPPC bilayers. A molecular dynamics and time-resolved fluorescence anisotropy study

Luís M.S. Loura [a,b,*], J.P. Prates Ramalho [a,c]

[a] Centro de Química and Departamento de Química, Universidade de Évora, Rua Romão Ramalho, 59, 7000-671 Évora, Portugal
[b] Centro de Química-Física Molecular, Complexo I, Instituto Superior Técnico, Av. Rovisco Pais, 1049-001 Lisboa, Portugal
[c] Centro de Física Teórica e Computacional, Av. Prof. Gama Pinto, 2, 1649-003 Lisboa, Portugal

Received 21 July 2006; received in revised form 9 October 2006; accepted 18 October 2006
Available online 27 October 2006

Abstract

100-ns molecular dynamics simulations of fluid 1,2-dipalmitoyl-*sn*-glycero-3-phosphocholine (DPPC) bilayers, both pure and containing 7-nitrobenz-2-oxa-1,3-diazol-4-yl (NBD) acyl-chain labeled fluorescent analogs (C6-NBD-PC and C12-NBD-PC), are described. These molecules are widely used as probes for lipid structure and dynamics. The results obtained here for pure DPPC agree with both experimental and theoretical published works. We verified that the NBD fluorophore of both derivatives loops to a transverse location closer to the interface than to the center of the bilayer. Whereas this was observed previously in experimental literature works, conflicting transverse locations were proposed for the NBD group. According to our results, the maximum of the transverse distribution of NBD is located around the glycerol backbone/carbonyl region, and the nitro group is the most external part of the fluorophore. Hydrogen bonds from the NH group of NBD (mostly to glycerol backbone lipid O atoms) and to the nitro O atoms of NBD (from water OH groups) are continuously observed. Rotation of NBD occurs with ~2.5–5 ns average correlation time for these probes, but very fast, unresolved reorientation motions occur in <20 ps, in agreement with time-resolved fluorescence anisotropy measurements. Finally, within the uncertainty of the analysis, both probes show lateral diffusion dynamics identical to DPPC.

Keywords: Fluorescence probes; NBD-labeled lipids; Molecular simulation; Membrane model system; Membrane penetration depth

1. Introduction

Fluorescence has been used as a major tool to study lipid bilayer structure for several decades now. Being natural lipids, with very few exceptions, nonfluorescent, fluorescence spectroscopy and microscopy techniques rely on the use of extrinsic membrane probes [1]. These can be lipophilic fluorophores of non-lipid nature (e.g., pyrene, diphenylhexatriene (DPH)), or design fluorophores linked to a lipid moiety.

Among the latter, a popular family is that of phospholipids labeled with the 7-nitrobenz-2-oxa-1,3-diazol-4-yl (NBD) fluorophore in one of the acyl chains (see [2] for a review). NBD derivatives are commercially available for all major phospholipid classes, and have been used extensively as fluorescent analogues of native lipids in biological and model membranes to study a variety of processes ([2–4]). As a fluorophore, NBD possesses convenient photophysical properties, such as good fluorescence quantum yield, environment sensitivity, and suitability for fluorescence resonance energy transfer experiments, as a donor (namely to rhodamine-based probes e.g., [5,6]) or acceptor, e.g., to DPH probes [7], and in homotransfer studies of lipid aggregation.

However, as with any extrinsic probe, two major points of concern arise when using NBD-acyl-chain-labeled lipids to report on membrane structure: The first, which will be addressed in this article, is the behaviour of the probe molecules inside the bilayer: what region of the bilayer is the probe

* Corresponding author. Centro de Química-Física Molecular, Complexo I, Instituto Superior Técnico, Av. Rovisco Pais, 1049-001 Lisboa, Portugal. Fax: +351 218464455.
E-mail address: pclloura@alfa.ist.utl.pt (L.M.S. Loura).

0005-2736/$ - see front matter © 2006 Elsevier B.V. All rights reserved.
doi:10.1016/j.bbamem.2006.10.011

sensitive to (that is, the probe transverse location) and its translational and rotational dynamics. The second point, which will be addressed elsewhere, is the magnitude of perturbation induced by the probe on the host lipid structure.

These questions are especially important given that the NBD moiety, if labeled at the end of an acyl chain, is prone to loop or "snorkel" to the water/lipid interface, due to the chromophore polarity and the acyl chain flexibility. This effect has been observed using both fluorescence and NMR spectroscopy, although its precise magnitude is not totally certain. By determining the rate constant for non-radiative excited-state decay, and taking into account its dependence on the local dielectric constant, Mazères et al. [3] proposed an external location, near the phosphate group. Fluorescence quenching data analyzed with the parallax method indicate an external location of 1-palmitoyl, 2-[12 -amino]dodecanoyl-*sn*-glycero-3-phosphocholine (C12-NBD-PC), about 1.9–2.0 nm from the center of 1,2-dioleyol-*sn*-glycero-3-phosphocholine bilayers (DOPC), and thus near the phosphate or even choline groups of the host lipids [8]. However, the same technique had previously yielded a much smaller value (1.22 nm, near the glycerol backbone/carbonyl lipid region) for C12-NBD-PC and its shorter *sn*-2 acyl chain relative 1-palmitoyl, 2-[6-NBD-amino]hexadecanoyl-*sn*-glycero-3-phosphocholine (C6-NBD-PC) in DOPC [9]. More recently, using NMR cross-relaxation rate measurements, Huster et al. [10] again obtained a location near the glycerol backbone/carbonyl region for both C12-NBD-PC and C6-NBD-PC, and a slightly more external location for the C12 derivative relative to the C6 counterpart was proposed (taking into account more efficient fluorescence quenching of the C12 probe by aqueous quencher dithionite).

Molecular dynamics (MD) simulations can be used to obtain detailed atomic-scale information on phospholipid bilayers [11,12]. MD Simulations of fluorescent probes DPH [13,14] and pyrene [15] in lipid membranes were recently reported. Although surprisingly few in number, these works showed the suitability of MD for calculation of a variety of properties of fluorescence probes in the bilayer, as well as their effect on the organization of the latter.

In the present study, we used 100-ns MD simulations of C6-NBD-PC and C12-NBD-PC in fluid phase 1,2-dipalmitoyl-*sn*-glycero-3-phosphocholine (DPPC) bilayers, to determine the transverse location of the fluorophore, as well as its preferred orientation in the membrane and translational and rotational dynamics. The results are compared with both literature experimental and theoretical data, and, for rotational dynamics, also original time-resolved fluorescence polarization measurements were carried out. The main findings of this work are: (i) the NBD moiety loops in the direction of the water/lipid interface. It has a broad transverse distribution in the bilayer, with a maximum located around the glycerol backbone/carbonyl region; (ii) NBD has a wide orientation range in the bilayer, the NO_2 group being the region of the fluorophore closest to the water/lipid interface; (iii) the NBD NH group is involved in hydrogen bonding to phospholipid glycerol backbone O atoms, and, for the case of C6-NBD-PC, these H bonds are predominantly intramolecular (whereas for C12-NBD-PC they are exclusively intermolecular); (iv) the theoretical rotational dynamics of the NBD group agree with the experimental fluorescence anisotropy decays, both pointing to average rotation correlation times of ~5 ns and (v) lateral translation diffusion coefficients of the NBD-PC probes are identical to that of the host lipid DPPC.

2. Materials and methods

2.1. Materials

1,2-Dipalmitoyl-*sn*-glycero-3-phosphocholine (DPPC, Fig. 1A), 1-palmitoyl-2-[6-(7-nitrobenz-2-oxa-1,3-diazol-4-yl)aminododecanoyl]-*sn*-glycero-3-phosphocholine (C6-NBD-PC, Fig. 1B) and 1-palmitoyl-2-[12-(7-nitrobenz-2-oxa-1,3-diazol-4-yl)aminododecanoyl]-*sn*-glycero-3-phosphocholine (C12-NBD-PC, Fig. 1C) were obtained from Avanti Polar Lipids (Birmingham, AL). 4-(2-hydroxyethyl)-1-piperazine sulfonic acid (HEPES), KOH and KCl (all from Merck, Darmstadt, Germany) were used to prepare the buffer solution 20 mM HEPES–KOH (pH 7.4). All organic solvents were of spectroscopic grade and came from Merck (Darmstadt, Germany). Deionized water was used throughout. All above materials were used without further purification. The concentrations of stock solutions of the probes were determined spectrophotometrically using ε(NBD-PC, 465 nm, in C_2H_5OH)=2.2×10^4 M^{-1} cm^{-1} [16].

2.2. Lipid vesicle preparation

Large unilamellar vesicles (LUV, ~100 nm diameter), containing the desired mole ratio of DPPC and NBD-PC, were prepared by extrusion of lipid dispersions through 100-nm pore diameter polycarbonate membranes as previously described [17]. The resulting lipid dispersions were stored at room temperature and used within 24 h of preparation. The concentrations of phospholipid stock solutions were determined using phosphate analysis [18].

2.3. Instrumentation

Absorption spectroscopy was carried out with a Jasco V-560 spectrophotometer. When necessary, absorption spectra were corrected for turbidity using the method of Castanho et al. [19]. Steady-state fluorescence measurements were carried out with an SLM-Aminco 8100 Series 2 spectrofluorimeter in a right angle geometry with the cell holder thermostated at the required temperature (±0.05 °C) using a circulating water bath. The light source was a 450 W Xe arc lamp and the reference was a Rhodamine B quantum counter solution. Correction of emission spectra was performed using the correction software of the apparatus. 5×5 mm quartz cuvettes were always used.

Fluorescence decay measurements were carried out with a time-correlated single-photon counting system, which is described elsewhere [20]. Excitation and emission wavelengths were 335 nm and 540 nm, respectively. Timescales were chosen for each sample in order to observe the decay through 2–3 intensity decades. Instrumental response functions for deconvolution were generated from a scattering dispersion (silica, colloidal water suspension, Aldrich, Milwaukee, WI).

Time-dependent fluorescence anisotropy, $r(t)$, is determined according to

$$r(t) = \frac{I_{VV}(t) - GI_{VH}(t)}{I_{VV}(t) + 2GI_{VH}(t)} \quad (1)$$

where I_{ij} are the steady-state vertical and horizontal components of the fluorescence emission with excitation vertical (I_{VV} and I_{VH}) and horizontal (I_{HV} and I_{HH}) to the emission axis. The correction for the eventual polarization dependence of the detection efficiency is given by the G factor ($G=I_{HV}/I_{HH}$), which, in our system, is equal to unity. Therefore, for calculation of $r(t)$, the intensity decays of polarized light $I_{VV}(t)$ and $I_{VH}(t)$ were obtained separately with the same accumulation time, and Eq. (1) was used with $G=1.00$.

The anisotropy decay parameters (rotational correlation times, ϕ_i, amplitudes, β_i, fundamental anisotropy, r_0, and residual anisotropy, r_∞) were determined using a global analysis method fitting simultaneously to the

vertically and horizontally polarized emission components, according to the expressions [21]:

$$I_{VV}(t) \otimes L(t) = \frac{1}{3} I(t)[1 + 2r(t)] \otimes L(t)$$
$$I_{VH}(t) \otimes L(t) = \frac{1}{3} I(t)[1 + r(t)] \otimes L(t) \quad (2)$$

where $I(t)$ is the intensity decay (obtained at the magic angle, 54.7 °), ⊗ denotes convolution and $L(t)$ the instrumental response function. The anisotropy decay was described by a sum of two exponentials (non-associative model), as follows:

$$r(t) = (r_0 - r_\infty)[\beta_1 \exp(-t/\phi_1) + \beta_2 \exp(-t/\phi_2)] + r_\infty \quad (3)$$

Data analysis was carried out using a non-linear least squares iterative convolution method based on the Marquardt algorithm [22]. The goodness of the fits was judged from the experimental χ^2 values, weighted residuals and autocorrelation plots.

2.4. Transition moment of NBD-PC

The UV-Vis absorption spectrum and dipole moment vector of the first allowed electronic transition of the NBD moiety of NBD-PC were calculated at the ZINDO-CI level, as implemented in ArgusLab 4.0.1 [23]. Water solvation was taken into account in the calculations by using the Self Consistent Reaction Field (SCRF). This calculation yielded λ = 477 nm for the wavelength of the first allowed electronic transition in water, in good agreement with typical experimental values for the absorption maximum of the NBD chromophore.

2.5. MD Simulations

Being the study object of this work the behaviour of individual fluorescence probe molecules in the bilayer (e.g., rotational and translational diffusion) rather than cooperative phenomena such as phase separation), MD runs were carried out over a long simulated time. In total, five 100-ns run of 64 phospholipid molecules and 1947 SPC water molecules were carried out. The choice of lipid system (DPPC at 323 K) enabled comparison to a plethora of published MD reports as well as experimental data (as discussed throughout the following section), enabling the validation of the MD parameterization. In one simulation, all phospholipid molecules were unlabeled DPPC. The starting configuration of this bilayer was downloaded from the Tieleman group web page (http://moose.bio.ucalgary.ca/files/dppc64.pdb). This file was the initial structure for most runs in [24] and stripped of the 1917 outermost water molecules, leaving still enough water content (water:lipid ratio = 32) for full bilayer hydration [25]. In two other simulations, one DPPC molecule was replaced by either a C6-NBD-PC or a C12-NBD-PC molecule. In two further simulations, four DPPC molecules were replaced by either four C6-NBD-PC or four C12-NBD-PC molecules (two in each bilayer leaflet in both cases). The latter runs are used in this work to improve statistics in the analysis of slow converging parameters (rotational and translational dynamics, see below) or infrequent events (atom–

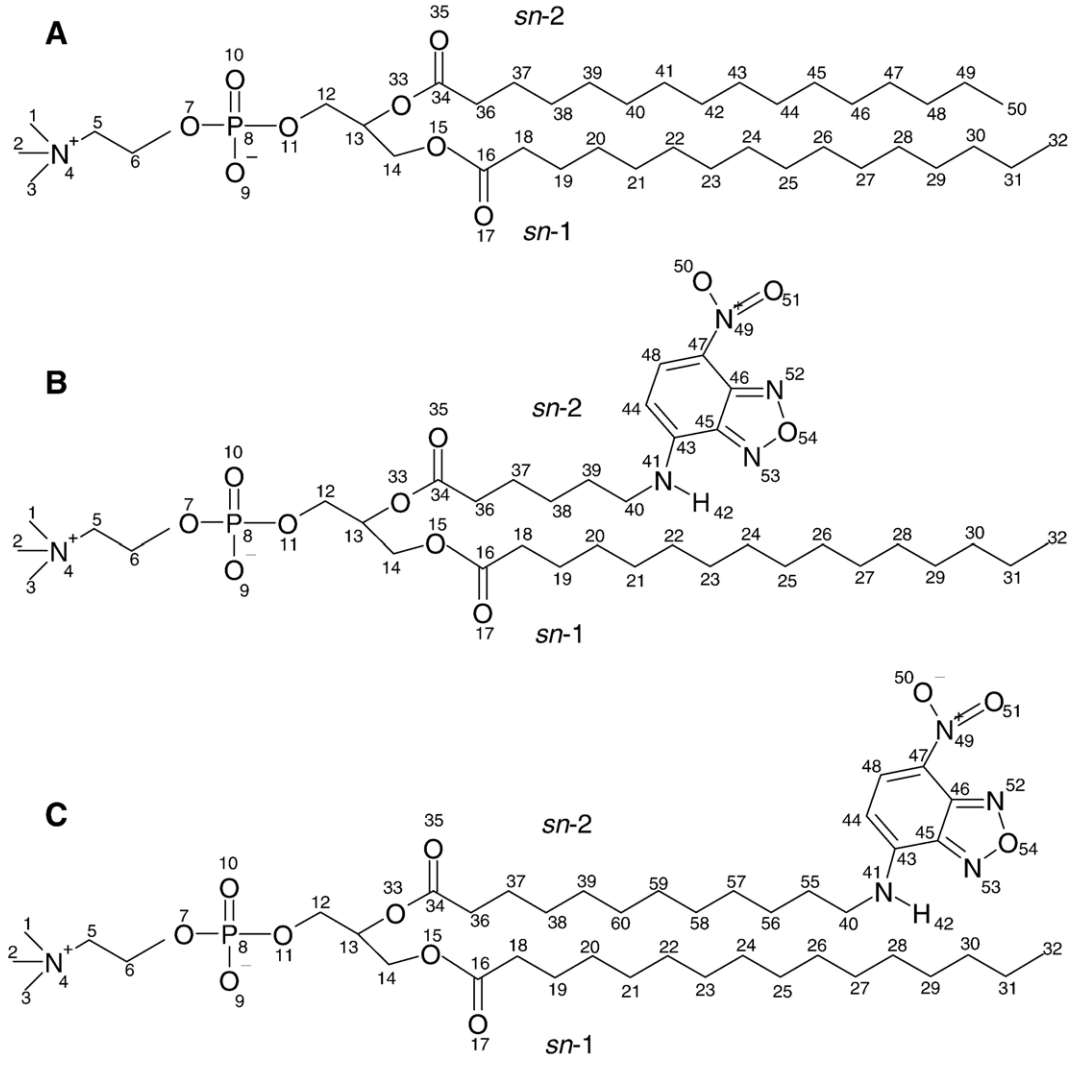

Fig. 1. Structures of (A) DPPC, (B) C6-NBD-PC and (C) C12-NBD-PC, showing the atom numbering as used throughout the text.

atom contacts, see below), and their complete analysis regarding NBD aggregation at high concentrations will be reported elsewhere.

All calculations were carried out with Gromacs 3.2 [26,27], under constant number of particles, pressure and temperature (323 K), and with periodic boundary conditions. Pressure and temperature control was carried out using the weak-coupling Berendsen schemes [28], with coupling times of 1.0 ps and 0.1 ps, respectively. Semiisotropic pressure coupling was used. All bonds were constrained to their equilibrium values, using the SETTLE algorithm [29] for water and the LINCS algorithm [30] for all other bonds. The robustness of this approach allowed the use of a time-step of 4 fs [31,32]. The long-range electrostatics Particle Mesh Ewald treatment [33] was applied, and van der Waals interactions were cut off at 0.9 nm [13,14]. Regarding the latter parameter, the use of 0.9 nm instead of a slightly higher value (say, 1.0 nm) might lead to a minor effect in the area per molecule, which, according to Repáková et al. [14] did not significantly affect the analysis of probe properties and probe-related effects in their studies of DPH-labeled DPPC membranes [13,14]. In all cases, the full 100-ns molecular dynamics simulations were preceded by an energy minimization run to eliminate overlaps, and a short (100 ps) MD run, similar to the full length simulation, except for the integration step (1 fs) and the pressure coupling time (2 ps).

Parameters for bonded and nonbonded interactions of the DPPC molecule were taken from [34] and are available at the GROMACS home page in http://www.gromacs.org/topologies/uploaded_force_fields/ffgmx_lipids.tar.gz. This force field uses united-atom description for CH, CH_2, and CH_3 groups. The partial charge distribution for DPPC in the underlying model, taken from http://moose.bio.ucalgary.ca/files/dppc.itp, was used. For the C6-NBD-PC and C12-NBD-PC molecules, parameters were based on those of DPPC, except for the fluorophore atoms (atoms 40–54, see Fig. 1B and C). For these, a preliminary topology was obtained using the PRODRG server [35]. Equilibrium bond lengths, angles and dihedrals were obtained through energy minimization carried out with the Gamess-US package [36,37]. Other parameters were taken from the OPLS all-atom forcefield [38]. Partial charges of the NBD group atoms were derived from ab initio quantum mechanical calculations [39] using Gamess-US and are given in Table 1. For water, the single-point charge (SPC) model was used [40].

3. Results and discussion

3.1. Area per phospholipid

Fig. 2 shows the time variation of the area per lipid molecule *a*, calculated as the instant box area divided by the number of lipid molecules in each monolayer (32), for pure DPPC bilayers (A), and 1:63 C6-NBD-PC:DPPC (B) or C12-NBD-PC:DPPC bilayers. The time variation of the area per lipid is a common indicator of the equilibration of the bilayer (e.g., [13]), whereas its average value is often used to assess the adequacy of the simulation methodology, due to its sensitiveness to simulation details [32]. Bearing this in mind,

Table 1
Atom charges (in units of *e*) derived from ab initio calculations for the NBD fluorophore (see text for details)

Atom number in Fig. 1	Partial charge/*e*	Atom number in Fig. 1	Partial charge/*e*
HCH40 (C6)	0.25	CH48	0.19
N41	−0.34	N49	0.86
H42	0.29	O50	−0.51
C43	−0.01	O51	−0.46
CH44	−0.12	N52	−0.30
C45	0.41	N53	−0.32
C46	0.41	O54	0.02
C47	−0.37		

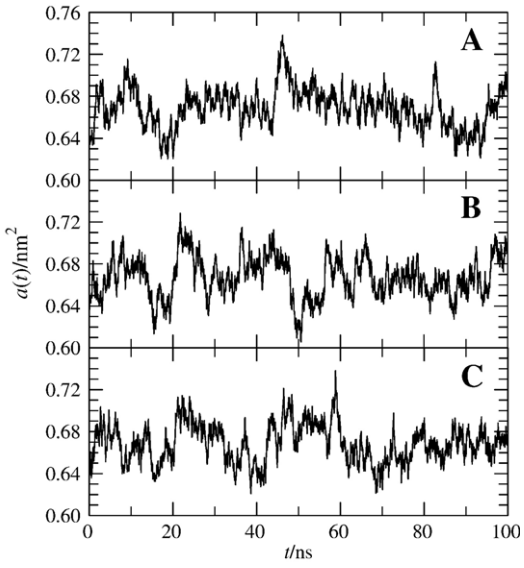

Fig. 2. Instant area/lipid molecule ($a(t)$) for (A) pure DPPC, (B) 1 C6-NBD-PC:63 DPPC and (C) 1 C12-NBD-PC:63 DPPC.

Fig. 2 shows that the initial configurations are close to equilibrium, and complete equilibration of our DPPC and 1:63 NBD-PC/DPPC bilayers was achieved in less than 10 ns. Therefore, unless specified otherwise, all further analyses were carried out using the last 90 ns of the full length simulations. On the other hand, the average values of for the simulations were $a = 0.669 \pm 0.004$ nm^2 for both DPPC and 1:63 C12-NBD-PC/DPPC and 0.667 ± 0.004 nm^2 for 1:63 C6-NBD-PC/DPPC, in very good agreement with both experimental (values from 0.56 to 0.71 nm^2 have been reported, with 0.64 nm^2 being regarded as a particularly precise estimate [41]) and theoretical [13,42–45] literature values for DPPC. Therefore, membrane labeling at 1:63 probe:total lipid ratio does not affect the average area/lipid molecule significantly.

It could be argued that replacement of a DPPC molecule in only one of the leaflets, by producing a membrane consisting of two leaflets of different composition, would potentially result in a mechanically unstable bilayer, leading, e.g., to increased fluctuations in the instantaneous molecular area. However, no such effect is apparent in the plots of Fig. 2, and the relative fluctuations in molecular area are identical for the DPPC, 1:63 C6-NBD-PC:DPPC and 1:63 C12-NBD-PC:DPPC simulations, as indeed for simulations of 4:60 C6-NBD-PC:DPPC and 4:60 C12-NBD-PC:DPPC symmetric bilayers (not shown).

3.2. Density profiles and transverse locations

Fig. 3 shows the mass density profiles across the bilayer obtained for water and DPPC for a pure DPPC bilayer, and compares them with those obtained for C6-NBD-PC (Fig. 3A) and C12-NBD-PC (Fig. 3B). Also shown are the profiles obtained for the NBD moiety (atoms 41–54 in Fig. 1B and C). To this effect, and because the bilayers' centers of mass may fluctuate in time, the positions of all atoms were determined relative to the instantaneous center of mass in all simulations, for each frame.

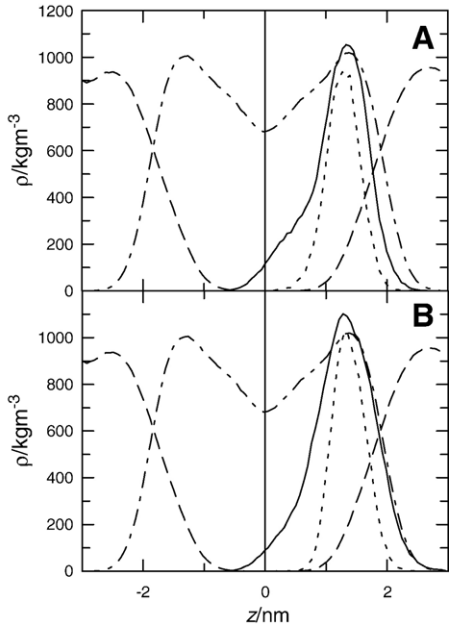

Fig. 3. Mass density profiles as a function of transverse position relative to the center of the bilayer (z). (A) Profiles of the C6-NBD-PC molecule (——) and the NBD fluorophore of C6-NBD-PC (atoms 41–54; - - - -) obtained in the 1 C6-NBD-PC:63 DPPC simulation. (B) Profiles of the C12-NBD-PC molecule (——) and the NBD fluorophore of C12-NBD-PC (atoms 41–54; - - - -) obtained in the 1 C12-NBD-PC:63 DPPC simulation. Additionally, both panels show the DPPC (– - – - –) and water (– – –) profiles obtained in the simulation of pure DPPC.

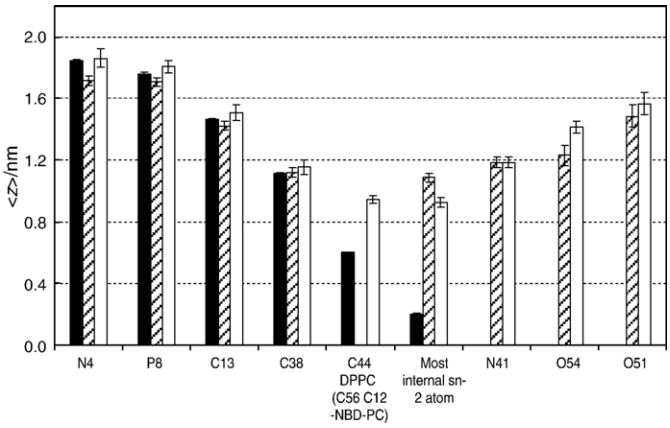

Fig. 4. Average distance from the bilayer center (<z>) for several atoms of DPPC (filled bars), C6-NBD-PC (shaded bars) and C12-NBD-PC (open bars). Error bars have two-standard-errors length. Most internal *sn*-2 chain atoms are C50, C39 and C57 for DPPC, C6-NBD-PC and C12-NBD-PC, respectively.

The results for DPPC profiles agree with those obtained from previous molecular dynamics reports [13,42–45]. The same can be said regarding the average positions of individual DPPC atoms along the bilayer normal (results not shown). As an example, the average position of C13 of DPPC, relative to the center of the bilayer, is found at $z=1.47$ nm, compared to $z \approx 1.55$ nm as reported in [13].

Similarly to all DPPC molecules, neither C6-NBD-PC nor C12-NBD-PC changed bilayer leaflet (flip-flop) during the simulation. As is apparent from the figure, the mass density profiles of the labeled phospholipids, despite being similar to each other, are rather distinct from that of DPPC. The most striking difference arises from the region close to the bilayer center ($z=0$), where the mass density of both C6-NBD-PC and C12-NBD-PC is largely reduced, despite the fact that the *sn*-2 chains of these molecules are heavier than those of DPPC. This is also not due to the asymmetrical distribution of C6-NBD-PC and C12-NBD-PC in the bilayer. It is clear that, even if there were a second labeled molecule, in the opposite leaflet, the added density in the $z \approx 0$ region would be nowhere as high as for DPPC. This is a first indication that the NBD fluorophore, which is attached to the end of the *sn*-2 chain, prefers a more shallow location in the bilayer than that to be expected solely from its position in the chain.

A more direct verification of this phenomenon is apparent from the average transverse position <z> of specific lipid atoms. Fig. 4 shows <z> for selected atoms along the DPPC (pure bilayer), C6-NBD-PC and C12-NBD-PC headgroup, glycerol backbone and *sn*-2 chains. The average z of the N4, P8 and C13 atoms is similar for the three species, being somewhat smaller (by 0.05–0.15 nm) for C6-NBD-PC in this region. Identical values for <z> are obtained for C38, the 4th carbon atom along the *sn*-2 chain, in all three species.

Further down the *sn*-2 chains, <z> falls to 0.203 nm (standard error 0.005 nm) for C50, the end atom of the *sn*-2 chain of DPPC. However, the atom with the deepest location in C6-NBD-PC is the 5th carbon atom (C39), with <z>=1.08 nm (standard error 0.03 nm). For C12-NBD-PC, the deepest atom of the *sn*-2 chain is the 9th carbon atom (C57), with <z>=0.92 nm (standard error 0.03 nm). For both molecules, all atoms of the NBD fluorophore are, on average, located closer to the water/lipid interface than these acyl chain atoms.

In any case, this study agrees with the recent observation, using NMR cross relaxation rates between a NBD ring proton and lipid protons, that the fluorophore is mainly located in the upper acyl chain/glycerol backbone region [10]. Although, as seen in Fig. 3, the NBD mass density profile obtained in this work is broad, it is not compatible with a preferential location of the fluorophore in the headgroup region, as reported in fluorescence studies (see Introduction). Our MD results allow the calculation of the number of "contacts" (distance <0.5 nm) between C44, the NBD CH group which contains the proton used in the NMR cross-relaxation experiment of Huster et al. [10] and specific DPPC atoms. This is shown in Fig. 5, where the results presented refer to simulations with four labeled phospholipids. Whereas no significant differences are obtained for the two derivatives, the similarity between these data and the experimental results of Huster et al. [10] is noteworthy.

Fig. 4 suggests that the NBD fluorophore is, on average, more distant from the bilayer center in C12-NBD-PC than in C6-NBD-PC. Interestingly, a slightly increased exposure of NBD to hydrophilic quencher dithionite for C12-NBD-PC relative to C6-NBD-PC was reported in 1-palmitoyl-2-oleoyl-*sn*-glycero-3-phosphocholine bilayers [10]. In the present study, for the center of mass of the NBD group, <z>=(1.38±0.05) nm and (1.31±0.05) nm are obtained for C12-NBD-PC and C6-NBD-PC, respectively. However, as seen from the standard errors, this difference is probably not significant. The NO_2 group is the

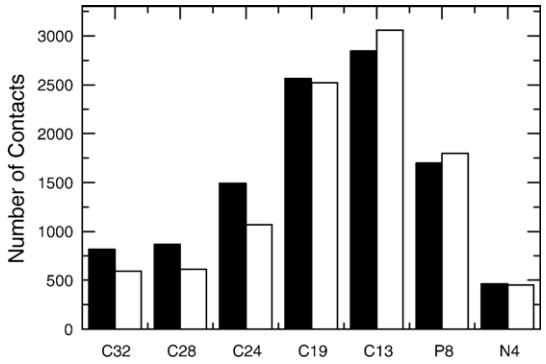

Fig. 5. Number of contacts (distance <0.5 nm), between NBD-PC C44 and specific DPPC atoms, registered during the simulation. Filled bars: C6-NBD-PC. Open bars: C12-NBD-PC.

region of the NBD moiety closest to the interface, with $\langle z \rangle =$ (1.50±0.07) nm and (1.44±0.07) nm for the centers of mass of these three atoms in C12-NBD-PC and C6-NBD-PC, respectively.

3.3. Order parameters

The "snorkelling" of the *sn*-2 chain of the NBD-PC probes is also evident from the variation of the deuterium order parameter S_{CD} across the acyl chain. S_{CD} is calculated for C atom i from $S_{CD,i} = -S_{zz,i}/2$, where

$$S_{zz,i}(i) = \left\langle \frac{1}{2}\left(3\cos^2\theta_{z,i} - 1\right) \right\rangle \quad (4)$$

in which $\theta_{z,i}$ is the angle between the vector uniting C atoms $i-1$ and $i+1$ and the bilayer normal (z axis; [46]). $-S_{CD}$ can vary between 0.5 (full order along the bilayer normal) and −0.25 (full order along the bilayer plane), whereas $S_{CD}=0$ denotes isotropic orientation. Fig. 6 shows $-S_{CD}$ for the *sn*-2 chain C atoms of DPPC, C6-NBD-PC and C12-NBD-PC. Due to the slow convergence of this parameter [47], analysis was restricted to the last 25 ns of the simulations. For the labeled species, and to better probe the chain orientation in the region close to the label, we included the N amine atom (N41) and the aromatic C bound to the latter (C43) in the chain for the sole purpose of S_{CD} calculation (theoretical S_{CD} values are thus calculated for 6 and 12 atoms, instead of 6−2=4 and 12−2=10 for the C6 and C12 derivatives, respectively.

The values calculated for DPPC show good agreement with those reported both in experimental ^{2}H-NMR works [48,49] and previous simulation studies [14,45,50]. Clear differences between DPPC and C12-NBD-PC are apparent from the 6th C atom onwards. $-S_{CD}$ becomes negative, and reaches a minimum of −0.17 for the 9th C atom, indicating a high degree of order of the 8th C atom–10th C atom vector along the bilayer plane. This is consistent with the above mentioned minimum of $\langle z \rangle$ for 9th C atom of this probe. For the remaining atoms of the chain, $-S_{CD}$ has again positive sign, and the very high calculated values for 12th C atom and the amino N atoms (0.28 and 0.36, respectively, considerably higher than for any DPPC acyl chain C atom) show that the end of the *sn*-2 chain which is linked to the NBD fluorophore is orderly oriented along the bilayer normal, antiparallel to the other end of the chain.

The short chain of C6-NBD-PC has a very different order profile to those described above. $-S_{CD}$ is positive for 2nd and 3rd C atoms, albeit smaller than for DPPC and C12-NBD-PC. In this region, the *sn*-2 chain is still oriented towards the center of the bilayer. For the remaining atoms, $-S_{CD}$ is negative, pointing to orientation along the bilayer plane rather than the bilayer normal of the end of the chain linked to the fluorophore.

3.4. Orientation of the NBD group

Fig. 7 shows the probability density functions $P(\theta)$ of the angles between the long axis (defined as the vector between atom O54 and the center of mass of atoms C44 and C48), the short axis (defined as the vector between atoms C45 and C46), and the normal to the NBD plane (defined as the vector product of the short and long axes) relative to the bilayer normal. For the short axis, similar $P(\theta)$ functions are recovered for both C6-NBD-PC and C12-NBD-PC. Both distributions are wide, but values $\theta > 90°$ predominate clearly (>75% for both derivatives), corresponding to C46 being closer to the interface than C45. Given the rigidity of the NBD moiety, this is a necessary consequence of the higher $\langle z \rangle$ obtained for the NO_2 group compared to the remainder of the fluorophore, as discussed above. For the long axis, $\theta < 90°$ predominates for C12-NBD-PC, corresponding to O54 being closer to the interface than the opposing end of this molecular axis. However, for C6-NBD-PC, a very wide distribution was recovered, which resulted from the observed possibility of jumps between conformations with either $\theta < 0°$ or $\theta > 90°$, and also conformations with $\theta \approx 90°$ (not shown). In any case, very similar $P(\theta)$ functions are obtained for the angle between the normal to the NBD plane and the bilayer normal. On the whole, the preferred orientations of the NBD group in C6-NBD-PC and C12-NBD-PC are similar. Fig. 8 shows typical snapshots of both molecules depicting these orientations, as well as the shallow location of the fluorophore discussed above.

3.5. Hydrogen bonds involving NBD atoms

The NBD fluorophore has an H atom bound to an amino N atom. This nitrogen can act as H-bond donor to water, DPPC, or

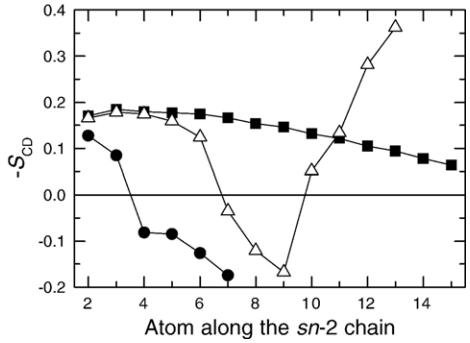

Fig. 6. Deuterium order parameter S_{CD} calculated for DPPC (■), C6-NBD-PC (●) and C12-NBD-PC (△) *sn*-2 chain atoms (for the two latter, the chain was extended to include N41 and C43 for calculation purposes; see text).

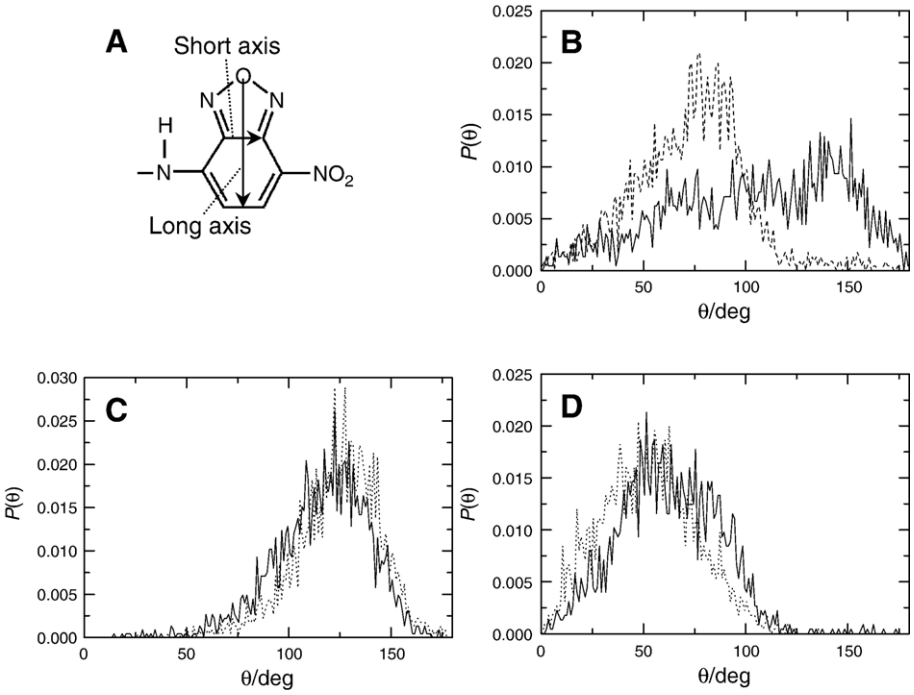

Fig. 7. (A) Definition of long and short axes of the NBD fluorophore. (B–D) Probability density functions $P(\theta)$ of the angles between the long axis (B), the short axis (C), and the normal to the NBD plane (defined as the vector product of the short and long axes; (D) relative to the bilayer normal. Solid lines: C6-NBD-PC. Dotted lines: C12-NBD-PC.

even C6-NBD-PC O atoms. On the other hand, there are several O and N atoms in the fluorophore, which can act as H-bond acceptors from water oxygen atoms. These interactions can be easily monitored in an MD simulation. For the following analysis, which used the last 80 ns of the simulations, a H-bond for a given donor–H–acceptor triad was registered each time the donor–acceptor distance is less than 0.35 nm.

Table 2 shows the frequency of H-bonding from N41 to each of the possible acceptor atoms. As seen from the totals, the NBD NH group is almost continuously involved in H-bonds. Note that due to the adopted definition of H-bonding, there can be more than one acceptor at the same time (if they are simultaneously located at a distance <0.35 nm to the NBD N41 atom), hence the totals can be higher than 100%, as verified for C6-NBD-PC. Low frequencies, in relative terms, are observed for both probes regarding H-bonding to water O atoms (4.4% for C6-NBD-PC; 4.9% for C12-NBD-PC) and H-bonding to phosphate O atoms (5.4% for C6-NBD-PC, including 3.8% intramolecular; 6.7% for C12-NBD-PC, entirely intermolecular). In both cases, H-bonding is most common to O atoms within the glycerol backbone, or (in the case of C6-NBD-PC, in which H-bonding to DPPC O16 atoms was observed for ~30% of the frames) to carbonyl O atoms. This correlates with the transverse location of the NBD group in the upper chain/glycerol region of the bilayer, as discussed above.

The most striking difference between the two derivatives is that, whereas for C12-NBD-PC all H-bonds to lipid atoms are intermolecular, for C6-NBD-PC most of them are intramolecular, to glycerol atoms O33 and O15 (46.7% and 13.5% of all H-bonds from N41, respectively). Intramolecular H-bonding to O33 and O15 is apparent in the snapshot shown in Fig. 8A. The combination of the short *sn*-2 chain of this species and the snorkeling of the NBD group results in proximity between the NH group and those glycerol backbone O atoms of the same molecule, facilitating H-bonding to the latter. For C12-NBD-PC, the bending of the longer *sn*-2 chain leads naturally to a much increased distance to the glycerol backbone O atoms of the same molecule, rendering intramolecular H-bonding impossible. However, as the transverse location of the NBD group is virtually identical to that of C6-NBD-PC, intermolecular H-bonding to DPPC glycerol backbone atoms has equally likely occurrence. This difference in H-bonding behavior, and the eventual distinct constraints posed by H-bonding on the conformation of the NBD fluorophore of the two derivatives, are probably a factor regarding the slight orientation differences analyzed in the preceding subsection.

Another way to look at this phenomenon is to compare the radial distribution of acceptor atoms around H42 of each probe. Fig. 9 shows radial densities $n(r)$ of O33 of NBD-PC and DPPC relative to H42 of NBD-PC, defined by

$$n(r) = \left\langle \frac{1}{N_{O33}} \sum_{j \in \{O33\}} \delta(r_j - r) \right\rangle_t = \frac{4\pi r^2 g(r)}{V} \quad (5)$$

In this equation, N_{O33} is the total number of acceptor atoms j (1 for NBD-PC, 63 for DPPC), V is the box volume, and $g(r)$ is the more commonly used radial distribution function. $n(r)$ was chosen in favor of $g(r)$ solely for the sake of representation (the information contained in both being obviously identical). Regarding the intramolecular $n(r)$ functions (Fig. 9A), there is a striking contrast between that of C6-NBD-PC, with its peak at

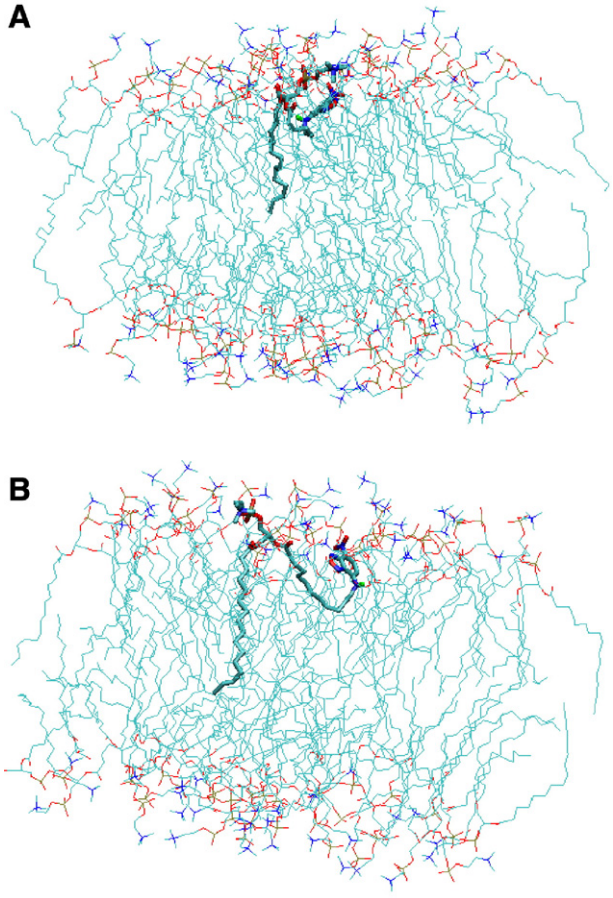

Fig. 8. Typical snapshots of C6-NBD-PC (A) and C12-NBD-PC (B) containing bilayers. Water molecules are omitted. CH_n groups (n=0–3), O atoms, N atoms and the NBD-PC H42 atom are shown in cyan, red, blue and green, respectively. Notice the intramolecular hydrogen bonds between N41-H42 of C6-NBD-PC and the oxygen atoms of the *sn*-2 chain.

$r \approx 0.16$–0.18 nm (typical of H-bonding), and that of C12-NBD-PC, where this peak does not exist, and there is only a very broad distribution in the 0.5 nm$<r<$1.5 nm range. On the other hand, the intermolecular $n(r)$ functions (Fig. 9B) are more similar, with that of C12-NBD-PC presenting the most intense

Table 2
N41-H42-acceptor atom H-bonds frequency

	C6-NBD-PC	C12-NBD-PC
Intramolecular	64.2 [a]	0.0
H_2O	4.4	4.9
DPPC phosphate	1.6	6.7
DPPC O15	0.3	21.5
DPPC O17	0.4	1.1
DPPC O33	0.9	60.2
DPPC O35	29.4	0.3
Total	101.2 [b]	94.8

The values indicate the percentage of frames (t >20 ns) for which N41 was H-bond donor to each of the described sets of atoms.

[a] 46.7% is due to N41-H42-O33 intramolecular H-bonding, 13.5% to N41-H42-O15 intramolecular H-bonding, and 3.8% to intramolecular H-bonding to phosphate O atoms.

[b] See text for explanation of total >100%.

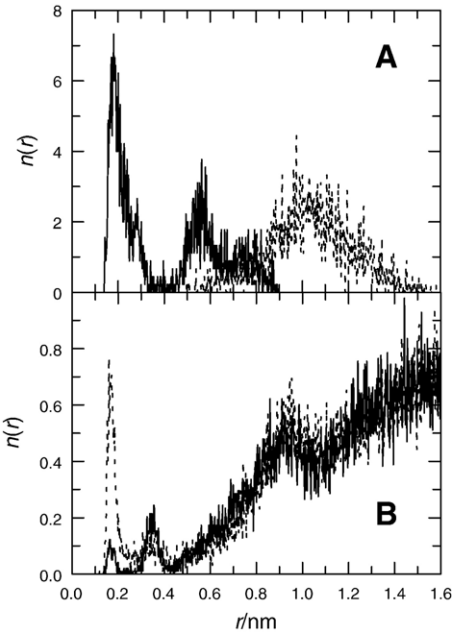

Fig. 9. Radial densities $n(r)$ (defined in Eq. (5) of O33 of NBD-PC (A) and DPPC (B) relative to H42 of C6-NBD-PC (solid lines) and C12-NBD-PC (dotted lines). Intramolecular hydrogen bonding predominates for C6-NBD-PC, whereas intermolecular hydrogen bonding predominates for C12-NBD-PC.

peak at H-bond distances, whereas that of C6-NBD-PC has a second clear peak at $r \approx 0.35$ nm, probably reflecting H-bonding of NBD H42 to the carbonyl O35 atom of DPPC.

Also of interest is H-bonding from water to N and O atoms of the NBD group, which, because of the well-known steep decrease of water penetration in the bilayer known to occur in this region (shown, e.g., in the density profile of Fig. 3), necessarily reflects the relative depth of each of these atoms in the membrane. Table 3 shows the average number of instant water O–water H–NBD acceptor triads during the last 80 ns of each run. It is clear that, of the NBD oxygen and nitrogen atoms, those which interact preferentially with water molecules are the nitro O atoms, O50 and particularly O51. The results for these atoms are even higher than the ones of the glycerol backbone atoms O33 and O15 in both molecules, which are also shown for comparison. This does not happen for any other N or O atom of the fluorophore, confirming that the NO_2 group is the most external part of the NBD moiety.

Table 3
Average number of instant H-bonds (registered for t >20 ns) between water O atoms (donor) and several specified NBD-PC atoms

NBD-PC Atom	Average number of H-bonds	
	C6-NBD-PC	C12-NBD-PC
O15	0.053	0.179
O33	0.107	0.270
N41	0.005	0.019
O50	0.375	0.313
O51	0.445	0.469
N52	0.044	0.099
N53	0.031	0.065
O54	0.041	0.102

3.6. Rotational dynamics of the NBD fluorophore

In order to study the rotational dynamics of the NBD fluorophore, a rotational autocorrelation function $C(t)$ was calculated, as defined below:

$$C(t) = \langle P_2(\cos\theta(\xi))\rangle \quad (6)$$

where $\theta(\xi)$, for the sake of commodity, is the angle between a vector defined in the molecular framework at times ξ and $t+\xi$, and $P_2(x)=(3x^2-1)/2$ is the second order Legendre polynomial. Averaging is performed over ξ, which assuming a sufficiently ergodic trajectory, is an approximation of the ensemble average. In any case, for this parameter, all shown analysis results are taken from the 4 NBD-PC:60 DPPC runs, and averaging over each NBD-PC molecule was carried out. This form of function can be compared with the fluorescence anisotropy decay, which for isotropic initial dipole distribution is given by [51,52]

$$r(t) = 0.4\langle P_2(\vec{\mu}_a(\xi)\cdot\vec{\mu}_e(t+\xi))\rangle \quad (7)$$

Here $\vec{\mu}_a$ and $\vec{\mu}_e$ are the normalized transition dipole moment vectors for absorption and emission, respectively. If one assumes that these vectors are approximately parallel, then r should have comparable time variation to that of $C(t)$ of the transition moment, apart from the 2/5 factor in the former.

To this purpose, the direction of the transition moment was estimated (see Materials and methods for computational details), and was found to be parallel (within 0.2°; not shown) to the NBD ring system short axis (vector uniting atoms C45 and C46). Therefore, this axis was used in all $C(t)$ calculations. Fig. 10A depicts the calculated $C(t)$ curves, whereas Fig. 10B shows the experimental fluorescence anisotropy decays. Fits of double-exponential decay functions were carried out to the simulated $C(t)$ functions, and deconvolution of the experimental $r(t)$ was carried out as described in Instrumentation. The best fit parameters are shown in Table 4, and the fitting functions are also depicted in Fig. 10 (note that comparison of the limiting values of $C(t)$ and $r(t)$ curves requires multiplying the former by 2/5)

From the MD simulations, it would be expected that the NBD fluorophore had very similar rotational dynamics in the C6 and C12 derivatives (Fig. 10A). However, judging from the experimental anisotropy decays, the measured decay rate of $r(t)$ of C12-NBD-PC is somewhat faster than that of C6-NBD-PC (Fig. 10B). In any case, our calculation of $C(t)$ still reflects the main features of the rotational dynamics of the NBD fluorophore in both probes as seen from the experimental $r(t)$:

(i) Average rotation correlation times are of the order of ~2.5–5 ns.

(ii) Two exponential components are required for adequate fits of both $r(t)$ and $C(t)$. The shorter correlation time is of the order of ~1 ns or less, whereas the longer one is in the 3–8 ns range. Although we did not study in detail the molecular origin of these exponential components, it is possible that the former might be related to rotational motion involving the NBD fluorophore, whereas the latter could arise from rotational motion of the whole NBD-PC molecule.

(iii) Small but finite residual values of $C(t)$ of C12-NBD-PC and $r(t)$ of both probes are observed at long times, that is, these functions have finite limits as $t\to\infty$. This is common for probes embedded in lipid bilayers, and may arise from "wobbling-in-cone"-type rotation [51]. In any case, these limiting values are low for the studied probes, indicating a relatively unhindered rotation. In this model for the anisotropy decay, the semi-cone angle for the wobbling of the emission dipole, θ_{max}, is related to the experimental r_∞/r_0 ratio through

$$\frac{r_\infty}{r_0} = \left[\frac{1}{2}(1+\cos\theta_{max})\cos\theta_{max}\right]^2 \quad (8)$$

Inserting the values obtained from analysis of $r(t)$ with Eq. (8) and shown in Table 4, one obtains $\theta_{max}=63°$ for C6-NBD-PC and 64° for C12-NBD-PC, in agreement with the broad angular distributions of the short axis shown in Fig. 7C.

(iv) From the best fit parameters of Table 4, it is clear that the values expected from these parameter sets for $t\to 0$ (C_0, r_0 for $r(t)$) fall short of the expected values of 1 for $C(t)$ and 0.4 for $r(t)$, being within 80–91% of them for $C(t)$

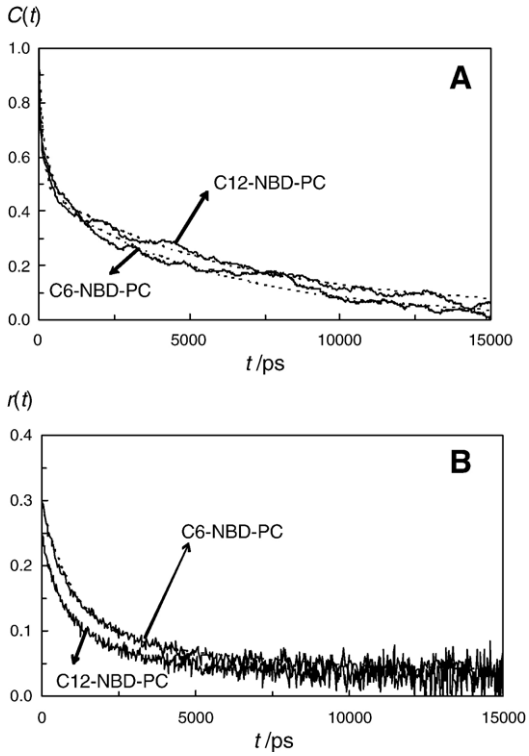

Fig. 10. (A) Autocorrelation functions $C(t)$ of NBD plane short axis (solid lines) and fits to double-exponential decay functions (dashed lines; parameters given in Table 4) for C6-NBD-PC and C12-NBD-PC. (B) Experimental anisotropy decays $r(t)$ of C6-NBD-PC and C12-NBD-PC (solid lines) and fits to Eq. (3) (dashed lines; parameters given in Table 4).

Table 4
Fitting parameters of the calculated rotational correlation functions $C(t)$ and experimental anisotropy decays $r(t)$, for C6-NBD-PC and C12-NBD-PC

	$C(t)=C_0\,[\beta_1\exp(-t/\phi_1)+\beta_2\exp(-t/\phi_2)]+C_\infty$		$r(t)=(r_0-r_\infty)[\beta_1\exp(-t/\phi_1)+\beta_2\exp(-t/\phi_2)]+r_\infty$	
Parameter	C6-NBD-PC	C12-NBD-PC	C6-NBD-PC	C12-NBD-PC
C_0 or r_0	0.80±0.02	0.91±0.02	0.290±0.005	0.297±0.006
β_1	0.41±0.02	0.49±0.02	0.77±0.02	0.55±0.02
ϕ_1/ns	0.33±0.02	0.13±0.01	1.15±0.05	0.34±0.02
β_2	0.59±0.01	0.51±0.01	0.23±0.02	0.45±0.02
ϕ_2/ns	5.7±0.1	6.3±0.2	8±1	3.2±0.2
$\langle\phi\rangle$/ns [a]	2.6	3.5	4.4	2.5
C_∞ or r_∞	0	0.036±0.003	0.031±0.001	0.030±0.001

[a] Calculated by integration of $C(t)$ or $(r(t)/0.4)$.

and 72–75% for $r(t)$. The somewhat lower value for $r(t)$ stems probably from nonparallel absorption and emission transition dipole moments. In any case, both results point to a very fast rotation component, which cannot be resolved in the time-scale used in both MD calculations and time-resolved polarized fluorescence measurements (that is, 20–40 ps time increments).

Overall, as seen in Fig. 10 and Table 4, there is fair agreement between the calculated $C(t)$ and the measured $r(t)$, especially given that the purpose of this work is not the exact theoretical calculation of $r(t)$ (as carried out in other systems in, e.g., [53,54]), but simply a rough comparison for validation of our MD model.

3.7. Lateral diffusion of NBD-PC

The lateral diffusion coefficients of the lipids were calculated from the two-dimensional mean square displacement (MSD), using the Einstein relation

$$D = \frac{1}{4}\lim_{t\to\infty}\frac{\mathrm{dMSD}(t)}{\mathrm{d}t}. \quad (9)$$

In turn, MSD is defined by

$$\mathrm{MSD}(t) = \langle||\vec{r}_i(t+t_0-\vec{r}_i(t_0)||)\rangle^2 \quad (10)$$

where $\vec{r}_i$ is the (x, y) position of the center of mass of molecule i of a given species, the averaging is carried out over all molecules of this kind, and $t_0=50$ ns is the chosen time origin for MSD calculation. To eliminate noise due to fluctuations in the center of mass of each monolayer, all MSD analyses were carried out using trajectories with fixed center of mass of one of the monolayers [32,55], and the final result is averaged over the two monolayers.

Fig. 11 shows MSD(t) for DPPC (pure bilayer), C6-NBD-PC and C12-NBD-PC (again both in 4 NBD-PC:60 DPPC bilayers, to improve statistics). Analyzing the final 50 ns of the simulations, diffusive two-dimensional translation was observed for all molecules. As seen in the figure, differences in MSD of the three species is not significant. In agreement, $D=(9.8\pm5.6)\times10^{-8}$ cm^2 s^{-1}, $(11.7\pm6.0)\times10^{-8}$ cm^2 s^{-1} and $(8.3\pm2.4)\times10^{-8}$ cm^2 s^{-1} were obtained for DPPC, C6-NBD-PC and C12-NBD-PC, respectively, all values being indistinguishable within the uncertainty of the calculations. The value for DPPC shows excellent agreement with published experimental results for this phospholipid above the main transition temperature, using techniques such as pulsed NMR [56], quasi-elastic neutron scattering [57] and a spin-label photobleaching method [58], as well as with published values from MD simulations [13,45,55].

Many techniques for determination of lateral diffusion coefficients in membranes either rely on the use of analog probes, or, albeit allowing the measurement of the diffusion coefficient of the bulk lipid species, are not suited to determination of D for a diluted analog probe. MD simulations can be easily used to determine simultaneously D for the probe and the host lipid, as illustrated here.

4. Concluding remarks

In this work, we present MD simulations of NBD-PC fluorescent analogs of phospholipid probes. The wide use of these molecules as probes for lipid structure and dynamics warrants these kind of studies. The results obtained for pure DPPC in this work, as discussed throughout this paper, agree with both experimental and theoretical published data, and validate our choices for MD parameters.

We found that the NBD fluorophore of NBD-PC adopts a transverse location closer to the water/lipid interface than to the center of the bilayer. This report helps to clarify a long standing doubt concerning the precise transverse location of the fluorophore. In agreement with an NMR study [10], and at variance with fluorescence reports [3,8], we found that the NBD group is mainly located in the upper acyl chain/glycerol backbone. For both derivatives, wide angular distributions of the fluorophore are apparent, and the nitro group is the most external part of the NBD moiety. Hydrogen bonds involving both the NH group of NBD as donor (and mostly the glycerol backbone lipid O atoms as acceptors) and the nitro O atoms of NBD as acceptors (from water OH donor groups) are continuously observed during the simulation time. The shorter chain of C6-NBD-PC favors the establishment of intramolecular H-bonds of NBD NH to lipid O atoms, which is not observed for

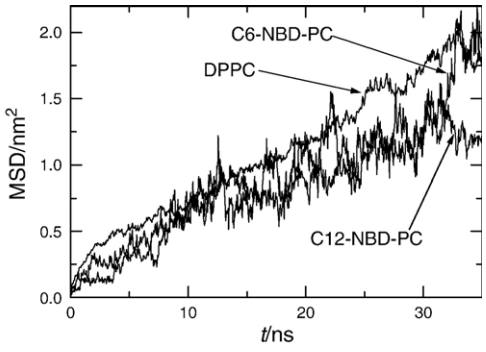

Fig. 11. Mean square displacement MSD(t) for DPPC in pure DPPC, C6-NBD-PC in 4C6-NBD-PC:60 DPPC, and C12-NBD-PC in 4C12-NBD-PC:60 DPPC simulations

C12-NBD-PC. Rotational reorientation of the NBD group occurs with ~2.5–5 ns average correlation time for both probes in this system, but very fast, unresolved reorientation motions occur in <20 ps, in agreement with time-resolved fluorescence anisotropy decays. Finally, within the uncertainty of the analysis, both probes show lateral diffusion dynamics identical to the host lipid.

In this work, we report on several features of isolated NBD-PC molecules in the bilayer. This is an essential first step in the characterization of the behavior of these widely used membrane probes. However, we are aware that a stringent test of the suitability of NBD-PC as a fluorescent analog of PC phospholipids also requires the study of the effects of the probes in the host lipid organization, as well as whether the former are uniformly distributed in the host bilayer or aggregate, and, in the latter situation, for what concentrations aggregation might occur. To this effect, further MD simulation analyses and fluorescence studies are underway, and will be presented in a forthcoming report.

Acknowledgements

The authors thank program POCI, FCT (Portugal) for funding and Dr. A. Fedorov for assistance in the time-resolved fluorescence experiments.

References

[1] L. Davenport, Fluorescence probes for studying membrane heterogeneity, Methods Enzymol. 278 (1997) 487–512.
[2] A. Chattopadhyay, Chemistry and biology of N-(7-nitrobenz-2-oxa-1,3-diazol-4-yl)-labeled lipids—fluorescent-probes of biological and model membranes, Chem. Phys. Lipids 53 (1990) 1–15.
[3] S. Mazères, V. Schram, J.F. Tocanne, A. Lopez, A, 7-nitrobenz-2-oxa-1,3-diazole-4-yl-labeled phospholipids in lipid membranes: differences in fluorescence behaviour, Biophys. J. 71 (1996) 327–335.
[4] S. Mukherjee, H. Raghuraman, S. Dasgupta, A. Chattopadhyay, Organization and dynamics of N-(7-nitrobenz-2-oxa-1,3-diazol-4-yl)-labeled lipids: a fluorescence approach, Chem. Phys. Lipids 127 (2004) 91–101.
[5] U. Marx, G. Lassmann, H.G. Holzhütter, D. Wüstner, P. Müller, A. Höhlig, J. Kubelt, A. Herrmann, Rapid flip-flop of phospholipids in endoplasmic reticulum membranes studied by a stopped-flow approach, Biophys. J. 78 (2000) 2628–2640.
[6] C. Leidy, W.F. Wolkers, K. Jørgensen, O.G. Mouritsen, J.H. Crowe, Lateral organization and domain formation in a two-component lipid membrane system, Biophys. J. 80 (2001) 1819–1828.
[7] L.M.S. Loura, A. Coutinho, A. Silva, A. Fedorov, M. Prieto, Structural effects of a basic peptide on the organization of dipalmitoylphosphatidylcholine/dipalmitoylphosphatidylserine membranes: a fluorescent resonance energy transfer study, J. Phys. Chem., B 110 (2006) 8130–8141.
[8] F.S. Abrams, E. London, Extension of the parallax analysis of membrane penetration depth to the polar-region of model membranes—Use of fluorescence quenching by a spin-label attached to the phospholipid polar headgroup, Biochemistry 32 (1993) 10826–10831.
[9] A. Chattopadhyay, E. London, Parallax method for direct measurement of membrane penetration depth utilizing fluorescence quenching by spin-labeled phospholipids, Biochemistry 26 (1987) 39–45.
[10] D. Huster, P. Müller, K. Arnold, A. Herrmann, Dynamics of membrane penetration of the fluorescent 7-nitrobenz-2-oxa-1,3-diazol-4-yl (NBD) group attached to an acyl chain of phosphatidylcholine, Biophys. J. 80 (2001) 822–831.
[11] W.L. Ash, M.R. Zlomislic, E.O. Oloo, D.P. Tieleman, Computer simulations of membrane proteins, Biochim. Biophys. Acta 1666 (2004) 158–189.
[12] H.L. Scott, Modeling the lipid component of membranes, Curr. Opin. Struct. Biol. 12 (2002) 495–502.
[13] J. Repáková, P. Čapková, J.M. Holopainen, I. Vattulainen, Distribution, orientation, and dynamics of DPH probes in DPPC bilayer, J. Phys. Chem., B 108 (2004) 13438–13448.
[14] J. Repáková, J.M. Holopainen, M.R. Morrow, M.C. McDonald, P. Èapková, I. Vattulainen, Influence of DPH on the structure and dynamics of a DPPC bilayer, Biophys. J. 88 (2005) 3398–3410.
[15] B. Hoff, E. Strandberg, A.S. Ulrich, D.P. Tieleman, C. Posten, ^{2}H-NMR study and molecular dynamics simulation of the location, alignment, and mobility of pyrene in POPC bilayers, Biophys. J. 88 (2005) 1818–1827.
[16] R.P. Haugland, Handbook of Fluorescent Probes and Research Chemicals, 6th ed.Molecular Probes, Eugene, OR, 1996.
[17] L.M.S. Loura, M. Prieto, Dehydroergosterol structural organization in aqueous medium and in a model system of membranes, Biophys. J. 72 (1997) 2226–2236.
[18] C.W. McClare, An accurate and convenient organic phosphorus assay, Anal. Biochem. 39 (1971) 527–530.
[19] M.A.R.B. Castanho, N.C. Santos, L.M.S. Loura, Separating the turbidity spectra of vesicles from the absorption spectra of membrane probes and other chromophores, Eur. Biophys. J. 26 (1997) 253–259.
[20] L.M.S. Loura, A. Fedorov, M. Prieto, Membrane probe distribution heterogeneity: a resonance energy transfer study, J. Phys. Chem., B 104 (2000) 6920–6931.
[21] J.R. Knutson, J.M. Beechem, L. Brand, Simultaneous analysis of multiple fluorescence decay curves — a global approach, Chem. Phys. Lett. 102 (1983) 501–507.
[22] D.W. Marquardt, An algorithm for least-squares estimation of non-linear parameters, J. Soc. Ind. Appl. Math. 11 (1963) 431–441.
[23] M.A. Thompson, ArgusLab 4.0.1 Seattle, WA Planaria Software LLC, 2004.
[24] S.J. Marrink, O. Berger, D.P. Tieleman, F. Jähnig, Adhesion forces of lipids in a phospholipid membrane studied by molecular dynamics simulations, Biophys. J. 74 (1998) 931–943.
[25] J.F. Nagle, R. Zhang, S. Tristram-Nagle, W. Sun, H.I. Petrache, R.M. Suter, X-ray structure determination of fully hydrated L alpha phase dipalmitoylphosphatidylcholine bilayers, Biophys. J. 70 (1996) 1419–1431.
[26] H.J.C. Berendsen, D. van der Spoel, R. van Drunen, GROMACS: A message-passing parallel molecular dynamics implementation, Comp. Phys. Comm. 91 (1995) 43–56.
[27] E. Lindahl, B. Hess, D. van der Spoel, GROMACS 3.0: A package for molecular simulation and trajectory analysis, J. Mol. Mod. 7 (2001) 306–317.
[28] H.J.C. Berendsen, J.P.M. Postma, A. DiNola, J.R. Haak, Molecular dynamics with coupling to an external bath, J. Chem. Phys. 81 (1984) 3684–3690.
[29] S. Miyamoto, P.A. Kollman, SETTLE: an analytical version of the SHAKE and RATTLE algorithms for rigid water models, J. Comp. Chem. 13 (1992) 952–962.
[30] B. Hess, H. Bekker, H.J.C. Berendsen, J.G.E.M. Fraaije, LINCS: A Linear Constraint Solver for molecular simulations, J. Comp. Chem. 18 (1997) 1463–1472.
[31] K.A. Feenstra, B. Hess, H.J.C. Berendsen, Improving efficiency of large time-scale molecular dynamics simulations of hydrogen-rich systems, J. Comput. Chem. 20 (1999) 786–798.
[32] C. Anézo, C.A.H. de Vries, D.P. Höltje, S.-J. Tieleman, Methodological issues in lipid bilayer simulations, J. Phys. Chem., B 107 (2003) 9424–9433.
[33] U. Essman, L. Perela, M.L. Berkowitz, T. Darden, H. Lee, L.G. Pedersen, A smooth particle mesh Ewald method, J. Chem. Phys. 103 (1995) 8577–8592.
[34] O. Berger, O. Edholm, F. Jahnig, Molecular dynamics simulations of a fluid bilayer of dipalmitoylphosphatidylcholine at full hydration, constant pressure, and constant temperature, Biophys. J. 72 (1997) 2002–2013.
[35] W. Schuettelkopf, D.M.F. van Aalten, PRODRG — a tool for high-throughput crystallography of protein–ligand complexes, Acta Crystallogr. D60 (2004) 1355–1363.

[36] M.W. Schmidt, K.K. Baldridge, J.A. Boatz, S.T. Elbert, M.S. Gordon, J.J. Jensen, S. Koseki, N. Matsunaga, K.A. Nguyen, S. Su, T.L. Windus, M. Dupuis, J.A. Montgomery, General Atomic and Molecular Electronic Structure System, J. Comput. Chem. 14 (1993) 1347–1363.
[37] M.S. Gordon, M.W. Schmidt, Advances in Electronic Structure Theory: GAMESS a Decade Later, in: C.E. Dykstra, G. Frenking, K.S. Kim, G.E. Scuseria (Eds.), Theory and Applications of Computational Chemistry, the first forty years, Elsevier, Amsterdam, 2005, pp. 1167–1189.
[38] W.L. Jorgensen, D.S. Maxwell, J. Tirado-Rives, Development and testing of the OPLS all-atom force field on conformational energetics and properties of organic liquids, J. Am. Chem. Soc. 118 (1996) 11225–11236.
[39] B.H. Besler, K.M. Merz, P.A. Kollman, Atomic charges derived from semiempirical methods, J. Comput. Chem. 11 (1990) 431–439.
[40] H.J.C. Berendsen, J.P.M. Postma, W.F. van Gunsteren, J. Hermans, Interaction models for water in relation to protein hydration, in: B. Pullman (Ed.), Intermolecular Forces, The Netherlands, Reidel, Dordrecht, 1981, pp. 331–342.
[41] J.F. Nagle, S. Tristram-Nagle, Structure of lipid bilayers, Biochim. Biophys. Acta 1469 (2000) 159–195.
[42] D.P. Tieleman, H.J.C. Berendsen, Molecular dynamics simulations of a fully hydrated dipalmitoyl phosphatidylcholine bilayer with different macroscopic boundary conditions and parameters, J. Chem. Phys. 105 (1996) 4871–4880.
[43] E. Falck, M. Patra, M. Karttunen, M.T. Hyvönen, I. Vattulainen, Lessons of slicing membranes: Interplay of packing, free area, and lateral diffusion in phospholipid/cholesterol bilayers, Biophys. J. 87 (2004) 1076–1091.
[44] S.W. Chiu, E. Jacobsson, R.J. Mashl, H.L. Scott, Cholesterol-induced modifications in lipid bilayers: A simulation study, Biophys. J. 83 (2002) 1842–1853.
[45] C. Hofsäß, E. Lindahl, O. Edholm, Molecular dynamics simulations of phospholipid bilayers with cholesterol, Biophys. J. 84 (2003) 2192–2206.
[46] R.B. Gennis, Biomembranes: Molecular Structure and Function, Springer-Verlag, New York, 1989.
[47] D.P. Tieleman, S.J. Marrink, H.J.C. Berendsen, A computer perspective of membranes: molecular dynamics studies of lipid bilayer systems, Biochim. Biophys. Acta 1331 (1997) 235–270.
[48] M.F. Brown, J. Seelig, U. Häberlen, Structural Dynamics in Phospholipid Bilayers From Deuterium Spin-Lattice Relaxation Time Measurements, J. Chem. Phys. 70 (1979) 5045–5053.
[49] H.I. Petrache, S.W. Dodd, M.F. Brown, Area per lipid and acyl length distributions in fluid phosphatidylcholines determined by 2H NMR spectroscopy, Biophys. J. 79 (2000) 3172–3192.
[50] M. Patra, M. Karttunen, M.T. Hyvönen, E. Falck, P. Lindqvist, I. Vattulainen, Molecular dynamics simulations of lipid bilayers: major artifacts due to truncating electrostatic interactions, Biophys. J. 84 (2003) 3636–3645.
[51] K. Kinosita, S. Kawato, A. Ikegami, A theory of fluorescence polarization decay in membranes, Biophys. J. 20 (1977) 289–305.
[52] T. Tao, Time-dependent fluorescence depolarization and Brownian rotational diffusion coefficients of macromolecules, Biopolymers 8 (1969) 609–632.
[53] P.A.W. van den Berg, K.A. Feenstra, A.E. Mark, H.J.C. Berendsen, A.J.W.G. Visser, Dynamic conformations of flavin adenine dinucleotide: simulated molecular dynamics of the flavin cofactor related to the time-resolved fluorescence characteristics, J. Phys. Chem. B. 106 (2002) 8858–8869.
[54] G.F. Schröder, U. Alexiev, H. Grubmüller, Simulation of fluorescence anisotropy experiments: probing protein dynamics, Biophys. J. 89 (2005) 3757–3770.
[55] E. Lindahl, O. Edholm, Molecular dynamics simulation of NMR relaxation rates and slow dynamics in lipid bilayers, J. Chem. Phys. 115 (2001) 4938–4950.
[56] A.L. Kuo, C.G. Wade, Lipid lateral diffusion by pulsed nuclear magnetic-resonance, Biochemistry 18 (1979) 2300–2308.
[57] S. König, W. Pfeiffer, T. Bayerl, D. Richter, E. Sackmann, Molecular-dynamics of lipid bilayers studied by incoherent quasi-elastic neutron-scattering, J. Phys. II 2 (1992) 1589–1615.
[58] J.R. Sheats, H.M. McConnell, Photo-chemical technique for measuring lateral diffusion of spin-labeled phospholipids in membranes, Proc. Natl. Acad. Sci. U. S. A. 75 (1978) 4661–4663.